Experimental and theoretical study of the *nf*-level lifetimes of potassium

M. Głódź,[1] A. Huzandrov,[1] M. S. Safronova,[2] I. Sydoryk,[1] J. Szonert,[1] and J. Klavins[3]
[1]*Institute of Physics, Polish Academy of Sciences, 02-668 Warsaw, Poland*
[2]*University of Delaware, Department of Physics and Astronomy, Newark, Delaware 19716 USA*
[3]*Institute of Atomic Physics and Spectroscopy, University of Latvia, 1586 Riga, Latvia*
(Received 18 October 2007; published 7 February 2008)

The theoretical and experimental values of the $5f$, $6f$, $7f$, and $8f$ radiative lifetimes τ of neutral potassium are reported. The reduced matrix elements for all allowed electric-dipole $nf_{5/2}$-$n'd_{5/2}$, $nf_{5/2}$-$n'd_{3/2}$, and $nf_{7/2}$-$n'd_{5/2}$ transitions with $n=5-8$ in K are calculated using the relativistic linearized coupled-cluster method with single and double excitations of Dirac-Fock wave functions included to all orders in many-body perturbation theory. The resulting electric-dipole matrix elements are used to evaluate the lifetimes of the $5f$, $6f$, $7f$, and $8f$ states in neutral K and their uncertainties. The contributions from the $nf_{5/2}$-$n'g_{7/2}$, $nf_{7/2}$-$n'g_{7/2}$, and $nf_{7/2}$-$n'g_{9/2}$ transitions to the lifetimes of the $6f$, $7f$, and $8f$ states are evaluated using the third-order many-body perturbation theory and are found to be very small. The theoretical results are $\tau_{5f}=117(4)$ ns, $\tau_{6f}=195(4)$ ns, $\tau_{7f}=301(6)$ ns, and $\tau_{8f}=441(9)$ ns. The experiment is performed in a cell using time-resolved fluorescence spectroscopy. The *nf* states are excited stepwise, $4s\rightarrow 4p\rightarrow nf$, using two pulsed synchronous dye lasers for the dipole and quadrupole transitions, respectively. The measured values $\tau_{5f}=117(3)$ ns, $\tau_{6f}=190(6)$ ns, $\tau_{7f}=309(8)$ ns, and $\tau_{8f}=428(10)$ ns are in excellent agreement with the present theoretical calculations.

DOI: 10.1103/PhysRevA.77.022503 PACS number(s): 32.70.Cs, 31.15.xp, 31.15.vj

I. INTRODUCTION

The radiative lifetimes of the excited states in neutral potassium have been the subject of many experimental studies [1–15] . Most of the studies focused on the measurements of the lifetimes of the low-lying excited states, especially the lowest *np* states, and few next following *ns*, *np*, and *nd* states [1–11]. Nevertheless, there were few experimental investigations of the potassium transition properties of higher excited states [12–15]. The radiative lifetimes of the $7s$-$11s$ and $5d$-$9d$ states of potassium have been measured by means of a time- and wavelength-resolved laser-induced-fluorescence approach by Gallagher and Cooke [12]. Relative transition probability measurements based on intensity measurements of optically thin K I spectral lines from a steady-state potassium emission source were reported for the *ns*-$4p$ ($n=6-15$), *nd*-$4p$ ($n=5-13$), and *nf*-$3d$ ($n=7-14$) series transitions by Aeschliman [13]. The relative accuracy was estimated to be 5–20 % for the *ns*-$4p$ and *nd*-$4p$ series and 15–25 % for the *nf*-$3d$ transitions [13]. The oscillator strengths of the $4s$-*np* lines of the principal series of potassium were determined by the Rozhdestvenskii hook method by Shabanova and Khlyustalov [14]. Radiative lifetimes of the (6–12)s, $(3-10)d_{3/2}$, and $(3-7)d_{5/2}$ states have been measured by time-resolved laser-induced fluorescence using two-photon excitation by Hart and Atkinson [15].

However, no experimental values appear to exist for the potassium *nf* state lifetimes. Our present measurements of K(*nf*) lifetimes with $n=5,6,7,8$ were aimed to partially fill this gap. Experiments with alkali *f*-states require some challenging attention to the choice of the excitation scheme owing to the difference in angular momentum quantum numbers $\Delta l=3$ between the *f* state and the ground n_0s state. In our experiment, we have applied the $4s\rightarrow 4p\rightarrow nf$ excitation scheme, with an electric quadrupole transition in the second step [16], similar to the one we used earlier for rubidium [17]. A review of other, more complex, schemes used by other authors to populate alkali *f*-state for lifetime measurement can be found in [17]. In these schemes, superradiant, or, in one case, microwave transitions were involved.

The theoretical calculations of a number of potassium transition properties were carried out using Coulomb approximation [18,19], Dirac-Fock method [20], and model potential [21,22]. The transition properties of a first few potassium states have been calculated with high precision using relativistic third-order perturbation theory including some higher-order correction [23], and using relativistic all-order method [24]. The most recent theoretical calculation of the K *nf* state lifetimes was performed in the mid-1980's by Theodosiou [22] using the model-potential method. There are no *ab initio* precision studies of the *f*-state transition properties for any of the alkali-metal atoms.

The motivation of this particular study is to conduct a benchmark test of the high-precision theoretical methods as well as provide accurate values of the *nf* state lifetimes and corresponding transition matrix elements. The all-order method used in this paper has been successfully applied to the calculation of the lifetimes of the low-lying states of the alkali-metal atoms and other systems with one valence electron [24,25]. It proved to be very successful in the calculation of the lifetimes of the lowest *np* levels, where high-precision experiments are available. So far, no test of the accuracy of the theoretical lifetimes of the states with such high values of the orbital angular momentum has been carried out. In this work, we have investigated possible issues that can arise in the all-order calculations of the *nf* state transition properties. The accurate calculation of the *nf* state properties is of interest, for example, for the calculation of the *nd* state light shifts in Ba^+ [26]. The properties of Ba^+ are of interest because of the parity nonconservation studies. The *nf*-*nd* transition properties are also needed for the evaluation

of the black-body radiation shifts for the clock transitions in the optical atomic clock schemes with monovalent ions. We find that our theoretical values are in excellent agreement with experimental measurements carried out in the present work.

II. THEORY

We calculate the 78 $nf_{5/2}$-$n'd_{3/2}$, $nf_{5/2}$-$n'd_{5/2}$, $nf_{5/2}$-$n'g_{7/2}$, $nf_{7/2}$-$n'd_{5/2}$, $nf_{7/2}$-$n'g_{7/2}$, and $nf_{7/2}$-$n'g_{9/2}$ reduced matrix elements in K that are needed for the evaluation of the $5f$, $6f$, $7f$, and $8f$ lifetimes. The nf-$n'd$ calculations are carried out using the relativistic all-order method that sums infinite sets of the many-body perturbation theory terms. The use of such high-precision method is necessary for the accurate evaluation of those lifetimes since some of the important matrix elements have very large correlation correction leading to poor convergence of the many-body perturbation theory. The particular all-order method used here is a linearized coupled-cluster method in which all single and double (SD) excitations of the Dirac-Fock wave function $|\Psi_v^{(0)}\rangle$ are included to all orders of perturbation theory. The SD all-order wave function for the state v of the monovalent system, such as K, is given by

$$|\Psi_v^{\mathrm{SD}}\rangle = |\Psi_v^{(0)}\rangle + \sum_{m\neq v} \rho_{mv} a_m^\dagger a_v |\Psi_v^{(0)}\rangle + \sum_{ma} \rho_{ma} a_m^\dagger a_a |\Psi_v^{(0)}\rangle + \frac{1}{2}\sum_{mnab} \rho_{mnab} a_m^\dagger a_n^\dagger a_b a_a |\Psi_v^{(0)}\rangle + \sum_{mna} \rho_{mnva} a_m^\dagger a_n^\dagger a_a a_v |\Psi_v^{(0)}\rangle. \quad (1)$$

The indexes a and b label the core states, while the indexes m and n label the excited states. We also conducted the all-order calculation with the partial inclusion of the most important triple excitations; the corresponding results are labeled "SDpT" in the text below. Only corrections due to triple valence excitation term

$$|\Psi_v^{\mathrm{SDpT}}\rangle = |\Psi_v^{\mathrm{SD}}\rangle + \frac{1}{6}\sum_{mnrab} \rho_{mnrvab} a_m^\dagger a_n^\dagger a_r^\dagger a_b a_a a_v |\Psi_v^{(0)}\rangle \quad (2)$$

are considered. Substituting the Eqs. (1), (2) into the many-body no-pair Hamiltonian yields the system of the all-order equations for the excitation coefficients ρ_{mv}, ρ_{ma}, ρ_{mmva}, ρ_{mnab}, and ρ_{mnrvab} as well as the correlation energy [27]. We did not include the equation for the triple excitation coefficients into the iteration procedure owing to the enormous computational resource requirements, but we considered the effect of the triples on the single valence excitation coefficients ρ_{mv} and correlation energy equations as described in Ref. [24]. The electric-dipole matrix elements are expressed as linear or quadratic functions of the SD excitation coefficients. We refer the reader to Refs. [24,25,27] for further description of the all-order method. Here, we describe specific challenges of the all-order calculations of the nf state lifetimes that are the subject of the present paper.

First, we use a finite basis set in all of the calculations that allows carrying out the sums over all possible excited states. The basis set used in the present calculations consists of the single-particle states, which are linear combinations of B splines [28]. The single-particle orbitals are defined on a nonlinear grid and are constrained to a spherical cavity. The cavity radius has to be large enough to accommodate all valence orbitals of interest. This requirement places a limit on a number of the excited states that can be accurately calculated with the all-order method since large cavity size requires the increasing number of the basis set states N to maintain the accuracy. Moreover, the required computations resources scale as N^2. As a result, the all-order calculations have been generally limited to a few excited states. The present calculation represents an excellent test of whether the boundary of the applicability of this method can be extended even to rather highly excited states with large orbital momentum. We tested the use of the various basis sets and concluded that $N=50$ basis set is large enough to produce accurate $8f$ and $7g$ wave functions while maintaining the good accuracy for the low-lying states with the cavity radius $R=190$ a.u. For comparison, the calculation of the $4s$ and $4p$ state properties in K requires the cavity of only 40 a.u. We also investigated the need for the denser grid and found that the denser grid was not needed for the accurate description of the higher excited states in the present case. These results represent rather remarkable findings of the all-order method stability for the calculation of the excited states with high values of the angular momentum. Secondly, we investigated the effect of the basis set truncation for the calculation involving the states with high values of the orbital angular momentum $l=3$. The basis set used in the calculation of the sums over the excited states has to be truncated at some value of the $l_{\max}$, generally $l_{\max}=6$, leading to either reduced accuracy for the states with higher l or the need for including the higher partial waves which is computationally demanding, especially for the heavier systems. The calculation of the f-state lifetimes in K represents an excellent case to investigate this issue. To study the effect of the higher partial waves on the nf-$n'd$ and nf-$n'g$ transitions, we have conducted two separate third-order many-body perturbation theory calculations such as described in Ref. [23]. One calculation was conduced with $l_{\max}=6$ and another one with $l_{\max}=9$. We found that the differences between these two calculations, which represent the contribution of the $l=7,8$, and 9, did not significantly exceed 1% even for the transitions where the correlation correction was very large. For most of the transitions, the difference was far below the estimated uncertainty of the correlation correction calculations resulting from the truncation of some triple and all quadrupole and higher excitations. Therefore, we found no need to increase the number of the partial waves in the all-order calculation. The third-order calculation, while rather complicated, requires by far fewer resources than the all-order one. We added the resulting third-order results for the $l=7$, 8, and 9 partial wave contributions to the $l_{\max}=6$ all-order values for all nf-$n'd$ transitions to account for the effect of the higher partial waves.

The contributions from the $nf_{5/2}$-$n'g_{7/2}$, $nf_{7/2}$-$n'g_{7/2}$, and $nf_{7/2}$-$n'g_{9/2}$ transitions to the lifetimes of the $6f$, $7f$, and $8f$ states are evaluated using the third-order many-body perturbation theory and are found to be very small. The correlation

correction contributions to these transitions are small (4%) and more accurate all-order calculation is not needed.

To make a comparison with the experiment, we also evaluated the uncertainty of our results. We investigated the following issues that affect the accuracy of the calculation of the relevant electric-dipole matrix elements: the relative size of the correlation correction (estimated as the difference between the lowest order and final results), the importance of the fourth- and higher-order terms (estimated as the difference between the third-order and all-order results), the importance of the triples excitations (estimated as the difference between the SD and SDpT calculations), and the breakdown of the various correlation correction terms. We found that there is a large variance in the size of the correlation correction and the relative importance of the higher-order terms for the nf-$n'd$ transitions with different n and n'.

We found triple excitations to be significant for a number of the transitions warranting further calculations. However, the study of the breakdown of the correlation correction showed that for all transitions, with the exception of the $6f$-$3d$ ones, only one term that contains only single excitations ρ_{mv} dominates. In the cases of the especially large correlation corrections (50%), this one term gives nearly the entire correction. We note that our SDpT approximation is especially aimed at correcting the single excitation coefficients ρ_{mv} making our SDpT *ab initio* calculations more reliable than the SD ones. To further estimate the effects of the omitted higher-excitation parts of the correlation correction, we conducted the scaling of the single-excitation coefficients for both SD and SDpT calculations. The scaling procedure is described in Refs. [24,25]. We found that the scaled SD and SDpT results are generally in much better agreement than the original SD and SDpT calculations, as expected. In the case of the $6f$-$3d$ transitions, two large correlation correction terms nearly cancel leading to a very small total correction. The SD *ab initio* and scaled data are nearly the same in this case.

We present the results for the $nf_{7/2}$-$n'd_{5/2}$ reduced matrix elements in K used in the calculation of the nf state lifetimes and their uncertainties in Table I. The lowest-order results are given to illustrate the size of the correlation correction. The SD scaled data are listed as the final results.

The uncertainty is calculated separately for each matrix element based on the uncertainty study described above. As we discussed, various numerical uncertainties are significantly below the uncertainty in the correlation corrections and can be entirely neglected. The uncertainty in the dominant correction is taken to be the largest of the differences between final results and *ab initio* SDpT and scaled SDpT results. The uncertainty in the remaining corrections should not exceed the uncertainty of the dominant term and is taken to be the same. The total uncertainty values are listed in Table I.

The lifetimes of the nf states are obtained as

$$\tau_v = \frac{1}{\sum_{w \le v} A_{vw}}, \tag{3}$$

where A_{vw} are the corresponding transition rates (Einstein A coefficients) [23]

TABLE I. The absolute values of the reduced electric-dipole matrix elements (a.u.) for the $nf_{7/2}$-$n'd_{5/2}$ transitions in K used in the calculation of the nf state lifetimes and their uncertainties. The lowest-order results are given to illustrate the size of the correlation correction.

Transition	Lowest order	Final	Uncertainty	
$5f_{7/2}$-$3d_{5/2}$	6.13	5.85	0.02	0.3%
$5f_{7/2}$-$4d_{5/2}$	20.5	15.4	1.0	7%
$5f_{7/2}$-$5d_{5/2}$	56.7	56.3	0.3	0.6%
$6f_{7/2}$-$3d_{5/2}$	3.48	3.45	0.02	0.6%
$6f_{7/2}$-$4d_{5/2}$	8.74	7.42	0.21	3%
$6f_{7/2}$-$5d_{5/2}$	24.5	16.2	1.8	11%
$6f_{7/2}$-$6d_{5/2}$	87.8	86.4	0.7	0.8%
$7f_{7/2}$-$3d_{5/2}$	2.36	2.38	0.02	1%
$7f_{7/2}$-$4d_{5/2}$	5.24	4.67	0.07	1.5%
$7f_{7/2}$-$5d_{5/2}$	11.06	8.43	0.45	5%
$7f_{7/2}$-$6d_{5/2}$	29.2	17.3	2.5	15%
$7f_{7/2}$-$7d_{5/2}$	124.1	121.2	1.1	0.9%
$8f_{7/2}$-$3d_{5/2}$	1.75	1.79	0.03	1.5%
$8f_{7/2}$-$4d_{5/2}$	3.65	3.34	0.03	0.8%
$8f_{7/2}$-$5d_{5/2}$	6.79	5.49	0.19	3.5%
$8f_{7/2}$-$6d_{5/2}$	13.43	9.35	0.69	7%
$8f_{7/2}$-$7d_{5/2}$	34.3	18.4	3.2	17%
$8f_{7/2}$-$8d_{5/2}$	165.6	161.0	1.6	1%

$$A_{vw} = \frac{2.02613 \times 10^{18}}{\lambda^3} \frac{|\langle w \| D \| v \rangle|^2}{2j_v + 1} s^{-1}. \tag{4}$$

In Eq. (4), $\langle w \| D \| v \rangle$ are the reduced electric-dipole matrix elements in a.u., λ is the transition wavelength in Å, and j_v is the total angular momentum of the state v. We list the transition rates $A_{vw}(10^6\ s^{-1})$ and their uncertainties for the transitions contributing to the $(5-7)f$ and $8f$ lifetimes in Tables II and III, respectively. The total sum $\Sigma_{w \le v} A_{vw}$ is given in the rows labeled "Total." The total uncertainties are obtained by adding the uncertainties of the individual contributions in quadrature. As expected, the $nf_{5/2}$ and $nf_{7/2}$ lifetimes are the same within the accuracy of our calculations.

We illustrate the importance of various contributions to lifetimes on the example of the $6f_{5/2}$ and $6f_{7/2}$ states. The $6f_{5/2}$-$3d_{3/2}$ and $6f_{7/2}$-$3d_{5/2}$ transitions give the dominant contributions to the $6f_{5/2}$ and $6f_{7/2}$ lifetimes, respectively. However, the contributions from the $6f_{5/2}$-$4d_{3/2}$ and $6f_{5/2}$-$5d_{3/2}$ transitions to the $6f_{5/2}$ lifetime and from the $6f_{7/2}$-$4d_{5/2}$ and $6f_{7/2}$-$5d_{5/2}$ transitions to the $6f_{7/2}$ lifetime are also very significant. The correlation corrections to these transitions are large, especially for the $6f$-$5d$ transitions, leading to the dominant contributions to the total uncertainty. The contributions from the $6f$-$5g$ matrix elements are small and their uncertainties are insignificant (the uncertainty in the corresponding matrix elements is taken to be 2% based on the study of the similar transitions). Our final theoretical results for the lifetimes obtained according to Eq. (3) as inverse of

TABLE II. Transition rates $A_{vw}(10^6\ s^{-1})$ and their uncertainties for the transitions contributing to the $5f$, $6f$, and $7f$ lifetimes.

Transition	$A_{vw}(10^6\ s^{-1})$	Transition	$A_{vw}(10^6\ s^{-1})$
$5f_{5/2}$-$3d_{3/2}$	6.04(4)	$5f_{7/2}$-$3d_{5/2}$	6.48(4)
$5f_{5/2}$-$4d_{3/2}$	1.86(26)	$5f_{7/2}$-$4d_{5/2}$	1.99(28)
$5f_{5/2}$-$5d_{3/2}$	0.0559(7)	$5f_{7/2}$-$5d_{5/2}$	0.0601(7)
$5f_{5/2}$-$3d_{5/2}$	0.432(3)		
$5f_{5/2}$-$4d_{5/2}$	0.133(18)		
$5f_{5/2}$-$5d_{5/2}$	0.00400(5)		
Total $5f_{5/2}$	8.53(26)	Total $5f_{7/2}$	8.53(28)
$6f_{5/2}$-$3d_{3/2}$	3.17(4)	$6f_{7/2}$-$3d_{5/2}$	3.40(4)
$6f_{5/2}$-$4d_{3/2}$	1.23(7)	$6f_{7/2}$-$4d_{5/2}$	1.32(7)
$6f_{5/2}$-$5d_{3/2}$	0.35(8)	$6f_{7/2}$-$5d_{5/2}$	0.37(8)
$6f_{5/2}$-$6d_{3/2}$	0.0300(5)	$6f_{7/2}$-$6d_{5/2}$	0.0322(5)
$6f_{5/2}$-$3d_{5/2}$	0.227(3)	$6f_{7/2}$-$5g_{7/2}$	0.00034(1)
$6f_{5/2}$-$4d_{5/2}$	0.088(5)	$6f_{7/2}$-$5g_{9/2}$	0.0120(5)
$6f_{5/2}$-$5d_{5/2}$	0.025(5)		
$6f_{5/2}$-$6d_{5/2}$	0.00215(3)		
$6f_{5/2}$-$5g_{7/2}$	0.0123(5)		
Total $6f_{5/2}$	5.13(11)	Total $6f_{7/2}$	5.13(12)
$7f_{5/2}$-$3d_{3/2}$	1.89(4)	$7f_{7/2}$-$3d_{5/2}$	2.03(4)
$7f_{5/2}$-$4d_{3/2}$	0.80(2)	$7f_{7/2}$-$4d_{5/2}$	0.85(3)
$7f_{5/2}$-$5d_{3/2}$	0.29(3)	$7f_{7/2}$-$5d_{5/2}$	0.31(3)
$7f_{5/2}$-$6d_{3/2}$	0.086(25)	$7f_{7/2}$-$6d_{5/2}$	0.092(26)
$7f_{5/2}$-$7d_{3/2}$	0.0160(3)	$7f_{7/2}$-$7d_{5/2}$	0.0172(3)
$7f_{5/2}$-$3d_{5/2}$	0.135(3)	$7f_{7/2}$-$5g_{7/2}$	0.00014(1)
$7f_{5/2}$-$4d_{5/2}$	0.057(2)	$7f_{7/2}$-$6g_{7/2}$	0.00033(1)
$7f_{5/2}$-$5d_{5/2}$	0.021(2)	$7f_{7/2}$-$5g_{9/2}$	0.0049(2)
$7f_{5/2}$-$6d_{5/2}$	0.006(2)	$7f_{7/2}$-$6g_{9/2}$	0.0116(5)
$7f_{5/2}$-$7d_{5/2}$	0.00115(2)		
$7f_{5/2}$-$5g_{7/2}$	0.0051(2)		
$7f_{5/2}$-$6g_{7/2}$	0.0119(5)		
Total $7f_{5/2}$	3.316(60)	Total $7f_{7/2}$	3.317(63)

the totals $\Sigma_{w\le v}A_{vw}$ listed in Tables II and III are $\tau_{5f}=117(4)$ ns, $\tau_{6f}=195(4)$ ns, $\tau_{7f}=301(6)$ ns, and $\tau_{8f}=441(9)$.

III. EXPERIMENT

A. Experimental setup and procedures

Each experimental potassium natural lifetime τ_{nf} was determined by analyzing decay of time-resolved $nf\rightarrow 3d$ fluorescence, resulting from pulsed selective excitation of the respective nf $(n=5,6,7,8)$ state. Excitation was carried out by synchronous pulses from two dye lasers via a two-step scheme $4s_{1/2}\rightarrow 4p_{3/2}\rightarrow nf_{5/2,7/2}$.

The scheme of the apparatus is shown in Fig. 1. The experiment was performed with a vapor over potassium droplet in a sealed off 1720 Corning glass cell. The cell, surrounded with double shield of high permeability foils to reduce external magnetic fields, was inserted into a temperature stabilized oven. The residual field was determined to be below

TABLE III. Transition rates $A_{vw}(10^6\ s^{-1})$ and their uncertainties for the transitions contributing to the $8f$ lifetimes.

Transition	$A_{vw}(10^6\ s^{-1})$	Transition	$A_{vw}(10^6\ s^{-1})$
$8f_{5/2}$-$3d_{3/2}$	1.23(4)	$8f_{7/2}$-$3d_{5/2}$	1.31(4)
$8f_{5/2}$-$4d_{3/2}$	0.539(9)	$8f_{7/2}$-$4d_{5/2}$	0.578(10)
$8f_{5/2}$-$5d_{3/2}$	0.21(2)	$8f_{7/2}$-$5d_{5/2}$	0.229(16)
$8f_{5/2}$-$6d_{3/2}$	0.084(13)	$8f_{7/2}$-$6d_{5/2}$	0.090(13)
$8f_{5/2}$-$7d_{3/2}$	0.027(9)	$8f_{7/2}$-$7d_{5/2}$	0.029(10)
$8f_{5/2}$-$8d_{3/2}$	0.0088(2)	$8f_{7/2}$-$8d_{5/2}$	0.0094(2)
$8f_{5/2}$-$3d_{5/2}$	0.088(3)	$8f_{7/2}$-$5g_{7/2}$	0.00007
$8f_{5/2}$-$4d_{5/2}$	0.0385(7)	$8f_{7/2}$-$6g_{7/2}$	0.00016(1)
$8f_{5/2}$-$5d_{5/2}$	0.015(1)	$8f_{7/2}$-$7g_{7/2}$	0.00025(1)
$8f_{5/2}$-$6d_{5/2}$	0.0060(9)	$8f_{7/2}$-$5g_{9/2}$	0.0025(1)
$8f_{5/2}$-$7d_{5/2}$	0.0019(7)	$8f_{7/2}$-$6g_{9/2}$	0.0055(2)
$8f_{5/2}$-$8d_{5/2}$	0.00063(1)	$8f_{7/2}$-$7g_{9/2}$	0.0088(4)
$8f_{5/2}$-$5g_{7/2}$	0.0026(1)		
$8f_{5/2}$-$6g_{7/2}$	0.0056(2)		
$8f_{5/2}$-$7g_{7/2}$	0.0090(4)		
Total $8f_{5/2}$	2.265(44)	Total $8f_{7/2}$	2.265(47)

10 mGs. We refer the reader to Ref. [29] for more detailed description of the cell and the oven. For each nf state, the measurements were performed at various temperatures. In the cell region of the laser excited fluorescence, the highest and lowest temperatures ever reached during the experiments were 377 and 441 K, respectively. The coldest end of the cell, with potassium droplet, was maintained at a temperature that was lower by 4–5 K. We applied Nesmeyanov formula

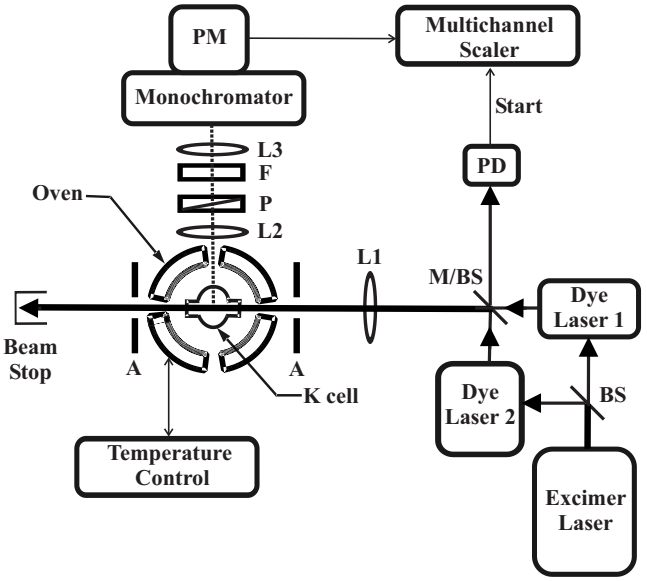

FIG. 1. Experimental setup. PM, photomultiplier; PD, photodiode; L1-L3, lenses; F, color glass filter; P, linear polarizer; A, alignment apertures; BS, beamsplitter; M/BS, wavelength-selective mirror or beam splitter (to combine the IR and visible light beams and to split a portion of the visible light beam from dye laser 1 towards the photodiode; see text for explanation of IR and visible light beams).

for temperature-vapor pressure relation [30]. The corresponding highest and lowest values of the potassium number density N in the excitation region were 2.9×10^{11} and 2.4×10^{13} cm^{-3}, respectively. The actual range of N values varied from state to state within this range.

Two pulsed dye lasers were pumped by a single Lumonics EX-520 excimer laser. To induce the $4s_{1/2}\rightarrow4p_{3/2}$ dipole transition, a beam at 766.5 nm (IR beam) was produced using a dye laser with 15 GHz linewidth. Lumonics HD-500 dye laser, with 4 GHz linewidth, was used for the $4p_{3/2}\rightarrow nf_{5/2,7/2}$ quadrupole transition, at 569.2. 528.7, 506.9, and 493.7 nm, for $n=5$, 6, 7, and 8, respectively (visible light beam). The combined beams were focused behind the oven with a long focal length lens. Inside the cell, the diameter of the overlapped beams was 0.4(1) mm in the region from where the fluorescence was observed. The IR and visible light pulses were synchronized for efficient excitation with an optical delay line, not represented in Fig. 1.

Both laser beams were vertically polarized. The fluorescence from the nf states was observed in the horizontal plane in the direction perpendicular to the laser beams through a polarizer set at 54.7° from the vertical orientation. In this way, a "magic angle" configuration was realized, and the decay of the flux of the observed fluorescence from the excited state is expected to be proportional to the decay of the state's population (e.g., Ref. [31]). Carl Zeiss Jena SPM2 grating monochromator was used to select a $nf\rightarrow3d$ fluorescence line, with fine structure (FS) unresolved, at 1102.1, 959.7, 890.3, or 850.4 nm, for $n=5,6,7$, or 8, respectively. The FS components of the lines are spanned by 0.3–0.2 nm. The strip of fluorescence emerging from the cell, parallel to the monochromator slits, was imaged (with reduction in size by a factor of 0.7) onto the entrance slit. The slits were set widely open to 1.5 mm to minimize thermal escape effect [32]. With such slit size, the effective spectral bandpass of the monochromator was 6 nm.

A photon-counting system including a photomultiplier and an EG&G PAR 914P multichannel scaler (MCS, 5 ns channel width) was used to register temporal development of fluorescence $I'_{nf}(t)$ (measurement a). In order to check and partially compensate for background counts in $I'_{nf}(t)$, after each $I'_{nf}(t)$ signal had been measured, a signal $I^{\mathrm{bg}}_{nf}(t)$ was collected under unchanged experimental conditions, such as the same cell temperature, laser power, etc., except that the visible light laser was detuned by 1 cm^{-1} from the $4p_{3/2}\rightarrow nf$ transition (measurement b). The difference $I_{nf}(t)=I'_{nf}(t)-I^{\mathrm{bg}}_{nf}(t)$ of signals normalized to the same number of laser shots was usually further processed. By subtracting $I^{\mathrm{bg}}_{nf}(t)$, we compensated for spurious counts from the sources common to measurements a and b, such as electronic noise (to the extent that sometimes such noise varied from measurement a to b) or photon counts of delayed fluorescence. The latter could originate e.g., in a cascade to nf from $(n+1)d$ state populated by ASE from visible light dye laser in a dipole $4p_{3/2}\rightarrow(n+1)d_{3/2,5/2}$ transition. Except for the noise from excimer laser electronics, registered in some initial channels of MCS, number of counts in $I^{\mathrm{bg}}_{nf}(t)$ was very small (with a tendency to decrease with time, i.e., with channel number), especially for the $n=5$ and 6 states.

A FEU 83 photomultiplier (S1 photocathode) was used for the $5f$ and $6f$ states, while Hamamatsu R943-02 photomultiplier (Ga-As photocathode) was used for the $7f$ and $8f$ states. The photocathodes were cooled to 200 and 250 K, respectively. A measure of the temporal resolution of the system is the 10 ns full width at half maximum of the laser pulse, as detected by the system. The actual length of the laser pulse, temporal response of the photomultiplier, and the temporal resolution of the multichannel scaler contributed to the effective pulse width.

For the $8f$ state, emission spectra were also registered to check for the presence of the fluorescence from some states other than the directly excited nf states in order to deduce possible effect of such states' population on the results. The $8f$ state was selected among the nf states of interest, as the one from which observed fluorescence lines were the closest to the lines of $4p\rightarrow4s$ fluorescence, and as the one most densely surrounded by the neighboring states. To register spectra, MCS was replaced by a two channel Stanford Research 430 photon counter. In the first channel, with the time-gate open from 100 to 600 ns following the moment of excitation, an "early spectrum" was registered, while in the second channel, with the gate open from 600 to 4000 ns a "delayed spectrum" was registered. The monochromator was tuned across near infrared, comprising the $8f$-$3d$ line and its neighborhood. The spectra were taken at some highest, lowest, and intermediate temperatures of the range used in the time-resolved study.

In the case of the $7f$ state, the $8p$-$5s$ spectral line lies only *ca* 2 nm apart from the observed $7f$-$3d$ line and, therefore, falls within spectral bandpass of the monochromator. Since the $7f$ state is connected to the $8p$ state by a cascade of the allowed $7f\rightarrow7d\rightarrow8p$ transitions, it was necessary to consider the effect of this coincidence on the $7f$ state lifetime measurements. An estimate, based on the branching ratios expected from Einstein coefficients and lifetimes taken from Ref. [19], shows that the number of photons in the $8p\rightarrow5s$ transition is only nearly 10^{-4} of the number of photons in the directly excited fluorescence $7f\rightarrow3d$ of interest. Therefore, the $8p\rightarrow5s$ fluorescence from the $8p$ state populated in a spontaneous emission cascade can be neglected. Some fast processes, such as superradiant cascades, observed earlier in alkali vapors [33,34] were also taken into consideration, as possibly feeding $8p$ population in a more efficient way after the $7f$ excitation. For laser-excited $8f$ state, $8f$-$3d$ and $9p$-$5s$ lines are around 11 nm apart and are resolvable. The inspection of the "early spectra" did not produce evidence for the presence of the $9p-5s$ line. By analogy, we expect absence of the $8p\rightarrow5s$ fluorescence with the excitation of the $7f$ state, especially that such conclusion is supported by unsuccessful trials of fitting two exponential functions to the $7f$ decay (see Sec. III B).

B. Data processing

In general, the time development of the fluorescence decay from the nf state in the presence of collisions could be a multiexponential function owing to the fine structure splitting of the nf state and the proximity of other nl states.

However, in the present experiment, single-exponential character of fluorescence decay is expected in view of our estimates which are based on the rate equations for population, similar to the ones discussed by, e.g., Pendrill [35] and Series [36]. The two-level rate equations of Pendrill and Series were supplemented by rates for collisional quenching out of the pair of the considered states. First, we have estimated that for each investigated nf state, the fast collisional j mixing within the very close in energy j substates of the FS doublet results in "immediate" statistical distribution of population among the j components; such statistical distribution is originally not accomplished in the mere act of excitation that proceeds via only one level (with $j=3/2$) of the $4p$ doublet. Secondly, another estimate shows that the effect of collisions leading to population of the states outside of the nf doublet can be considered as merely unidirectional quenching of each state nf_j, with the rate $R^{\mathrm{q}}_{nf_j}=\sigma^{\mathrm{q}}_{nf_j}N\upsilon$, and the backstream repopulating the nf state can be disregarded. The symbol $\sigma^{\mathrm{q}}_{nf_j}$ designates a cross section for collisional quenching to all states except the other doublet component. N is the number density of the ground state atoms and $\upsilon=(8kT/\pi\mu)^{1/2}$ is the mean relative velocity of the colliding partners (excited-state and ground-state K atoms), where μ is their effective mass. In this estimate, only the other states of the same hydrogenlike n-manifold, i.e., $nl>3$ states were taken into consideration for each nf doublet. These states are predominantly populated in nf doublet collisional quenching because they are its closest and the highest multiplicity neighbors. Finally, the light emitted in all three $nf_j \rightarrow 3d_{j'}$ transitions was detected unresolved for each n. Therefore, the observed fluorescence is expected to decay as a single exponential function with the decay parameter (rate) Γ_{nf} being the statistical average

$$\Gamma_{nf}=(g_{5/2}\Gamma_{nf_{5/2}}+g_{7/2}\Gamma_{nf_{7/2}})/(g_{5/2}+g_{7/2}), \tag{5}$$

where $g_j=2j+1$ is the statistical weight of a j component. For each nf_j, $\Gamma_{nf_j}=1/\tau^{\mathrm{rad}}_{nf_j}+R^{\mathrm{q}}_{nf_j}=1/\tau^{\mathrm{rad}}_{nf_j}+\sigma^{\mathrm{q}}_{nf_j}N\upsilon$, where $\tau^{\mathrm{rad}}_{nf_j}$ is the radiative lifetime of the component. The rate Γ_{nf} can be expressed in terms of respective statistical averages $1/\tau^{\mathrm{rad}}_{nf}$ and σ^{q}_{nf} as

$$\Gamma_{nf}=1/\tau^{\mathrm{rad}}_{nf}+\sigma^{\mathrm{q}}_{nf}N\upsilon, \tag{6}$$

where $1/\tau^{\mathrm{rad}}_{nf}$ and σ^{q}_{nf} are defined by rates for respective fine-structure components, $1/\tau^{\mathrm{rad}}_{nf_j}$ and σ_{nf_j}, just as the average rate Γ_{nf} is expressed in Eq. (5) in terms of the rates Γ_{nf_j}.

Radiative lifetime τ^{rad}_{nf} is shortened in comparison with the natural lifetime τ_{nf} because of the blackbody radiation (BBR) present in the cell, which induces transitions depopulating nf state with the rates $\Gamma^{\mathrm{BBR}}_{nf}$, depending on the cell temperature:

$$1/\tau^{\mathrm{rad}}_{nf}=1/\tau_{nf}+\Gamma^{\mathrm{BBR}}_{nf}. \tag{7}$$

For a given nf state, Γ_{nf} values corresponding to each temperature setting of the experiment (i.e., to each $N\upsilon$ value) were obtained as described below.

A single exponential function

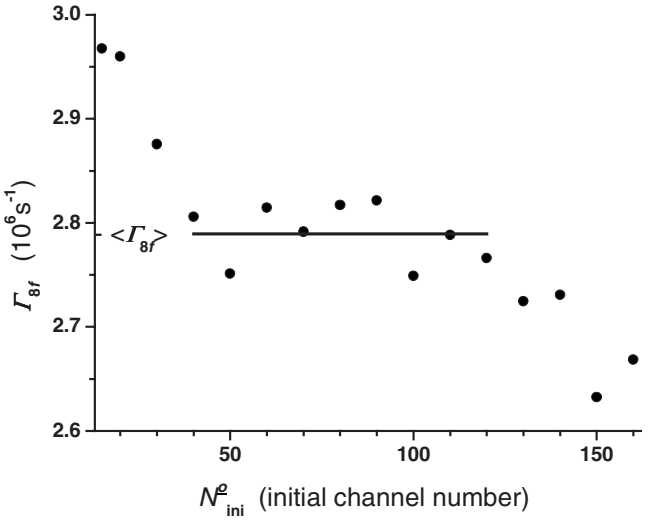

FIG. 2. An example of a plot of fitted values of the rates Γ_{nf} vs the initial channel number N^o_{ini} of a decay with successively truncated beginning. The straight line at the value $\langle\Gamma_{8f}\rangle$ represents the mean over a selected range of N^o_{ini}, in which systematic dependence of Γ_{nf} on N^o_{ini} is not observed. Mean value obtained in such a way was taken to be the result of a fitting procedure applied to a fluorescence decay (here from the $8f$ state) accumulated at a given temperature of the cell. The departure from $\langle\Gamma_{8f}\rangle$ outside of both its ends of the line suggests that in this measurement, an uncompensated background made a significant contribution to the fitted Γ_{8f} value, both in a considerable range of the initial channels and in the remote channels.

$$I_{nf}(t)=I^0_{nf}\exp(-\Gamma_{nf}t)+\alpha \tag{8}$$

was numerically fitted to experimental fluorescence decay signal from which the respective background signal $I^{\mathrm{bg}}_{nf}(t)$ was subtracted. Constant α was usually treated as a free parameter and was added to compensate for possible change in the time-independent portion of the noise between measurements a and b. It was also meant to approximate other, weakly depending on time, uncompensated "backgrounds," which do not appear or are smaller when the laser is off-resonance. The example of such background is photon counts originating, e.g., in two-photon ionization by visible light laser, followed by recombination to higher atomic states connected with the given nf state by a fluorescence cascade. For each experimental decay, the fit was repeated several times, with the initial part of the decay being successively truncated, in steps of 5 or 10 channels. An example of the plot of the resulting Γ_{nf} values versus the initial channel number $N^{\mathrm{o}}_{\mathrm{ini}}$ is shown in Fig. 2. Such plots were analyzed to select a range of $N^{\mathrm{o}}_{\mathrm{ini}}$ (40–120 in Fig. 2), in which fitted Γ_{nf} do not exhibit a systematic dependence on N^o_{ini}. A value $\langle\Gamma_{nf}\rangle$, a mean from such range (straight line in Fig. 2) was considered to be the result of a particular fitting procedure. An average of two $\langle\Gamma_{nf}\rangle$ results of such procedure performed with an experimental decay truncated to two different end channels was taken as a final result $\langle\langle\Gamma_{nf}\rangle\rangle$ for a decay registered at a certain temperature for the states with $n=5-7$.

For the $8f$ state, both $I^{\mathrm{bg}}_{nf}(t)$ signal and fitted α were most pronounced, the latter indicating presence of a somewhat el-

evated uncompensated background. Therefore, the above described fitting procedure was supplemented for the $8f$ state by a similar one, but with the fitting function being a sum of two single exponential functions

$$I_{nf}(t) = I_{nf}^0 \exp(-\Gamma_{nf} t) + I_b^0 \exp(-\Gamma_b t) + \alpha. \quad (9)$$

The second exponential function was meant to approximate the time dependence of the long-lasting backgrounds. In this procedure, $I_{nf}^{\mathrm{bg}}(t)$ was not subtracted and α (practically 0) was taken to be an average content of very remote channels. Γ_b was either treated as a free parameter or as a fixed value, which was deduced from the time dependence of I_{8f}^{bg}, approximated by a single exponential function. In both cases, fitted I_b^0 was found to be no more than *ca* 1% of fitted I_{8f}^0. The inverse of fitted Γ_b parameter characterizing the long-decay component slowly increased with truncating the initial channels as expected for composite delayed background, while the Γ_{8f} rate of interest did not exhibit systematic changes within a certain range of N_{ini}^o values. A mean from such range $\langle\Gamma_{8f}\rangle$ was taken as a result of the fit, as it was in the case of single exponential fitting. The two resulting $\langle\Gamma_{8f}\rangle$ values were found to be close to each other and to the ones obtained with function (8). The latter were obtained by fitting procedures with different end channel number and/or with α treated either as free parameter, or as a mean from the remote channels. An average $\langle\langle\Gamma_{8f}\rangle\rangle$ of the results of all fitting approaches with functions (8) and (9) was taken to be the final result corresponding to a certain temperature of the cell.

In the case of the $7f$ state, the double exponential fitting failed. As mentioned in Sec. III A, such fitting was performed for this state to check the possible influence of the $8p \rightarrow 5s$ fluorescence on the Γ_{7f} result. No systematic and reasonable values for second rate, Γ_b in formula (9), was obtained from the fitting procedure, neither in the case where both Γ_{7f} and Γ_b were treated as free parameters, nor when Γ_b was fixed at the value $\Gamma_b \approx 1/\tau_{8p}$, with τ_{8p} taken from Ref. [22]. This result is in agreement with the earlier conclusion drawn from the fact that since no $9p \rightarrow 5s$ fluorescence was discovered in the "early spectra" produced with $8f$ state directly excited, there is no $8p \rightarrow 5s$ fluorescence when the $7f$ state was excited (see Sec. III A).

Hereafter, the symbols of averaging are omitted for simplicity, and we use the symbol Γ_{nf} for final averaged values named above as $\langle\langle\Gamma_{nf}\rangle\rangle$. The respective $\Gamma_{nf}^{\mathrm{BBR}}$ value corresponding to the temperature T of the excitation region of the potassium cell of the particular decay measurement was subtracted from each such final result Γ_{nf} to correct for the effect of thermal radiation

$$\Gamma_{nf}^{\mathrm{corr}} = \Gamma_{nf} - \Gamma_{nf}^{\mathrm{BBR}}. \quad (10)$$

Corrections due to thermal radiation were taken from Ref. [22] and interpolated to the temperature values T. The $\Gamma_{nf}^{\mathrm{BBR}}$ rates were estimated to be 0.3–0.5 %, 1.0–1.3 %, 2.1–2.4 %, 2.4–3.3 % of Γ_{nf}, for $n=5$, 6, 7, 8, respectively.

The resulting values $\Gamma_{nf}^{\mathrm{corr}}$ are plotted in Fig. 3 as a function of $N\upsilon$ (Stern-Volmer plots). The linear dependence of $\Gamma_{nf}^{\mathrm{corr}}$ on $N\upsilon$ is expected $\Gamma_{nf}^{\mathrm{corr}} = 1/\tau_{nf} + \sigma_{nf}^{\mathrm{q}} N\upsilon$ (a Stern-Volmer relation) from Eqs. (6), (7), and (10). By fitting the Stern-Volmer relation to the experimental dependence, the natural lifetime τ_{nf}, being an inverse of a collisionless limit of $\Gamma_{nf}^{\mathrm{corr}}$ at $N\upsilon=0$, as well as collisional quenching cross section σ_{nf}^{q} were obtained (for σ_{nf}^{q} values see Ref. [37]). The contribution of each experimental point to the minimized χ^2 function was weighted by the inverse of the square of the uncertainty in Γ_{nf}, and standard deviation of the decay rates subject to final averaging was usually adopted for this uncertainty represented by Γ_{nf}-error bars on the plots in Fig. 3.

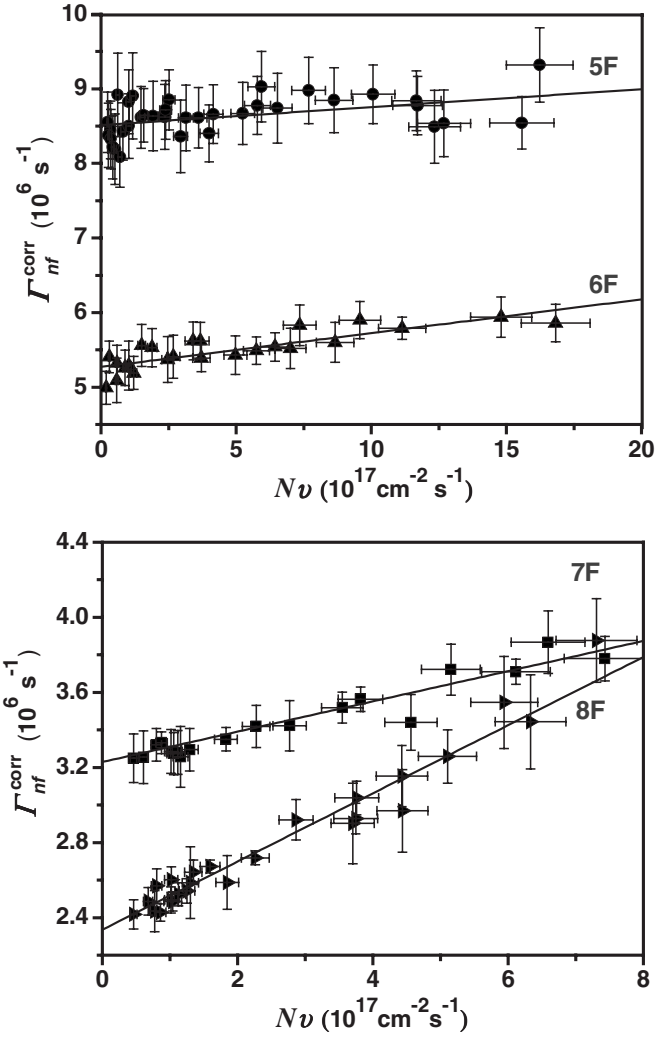

FIG. 3. Stern-Volmer plots for the nf states, in pairs for $n=5,6$ and $n=7,8$ states. The $\Gamma_{nf}^{\mathrm{corr}}$ values, which are the averaged experimental decay rates corrected for the effect of thermal radiation present in the cell, are plotted versus $N\upsilon$ (N is the number density of K atoms and υ is the mean relative velocity of the colliding partners). The straight lines are fits to Stern-Volmer relation $\Gamma_{nf}^{\mathrm{corr}} = 1/\tau_{nf} + \sigma_{nf}^{\mathrm{q}} N\upsilon$, with natural lifetimes τ_{nf} and collisional quenching cross sections σ_{nf}^{q} treated as free parameters.

For the lifetime uncertainty, twice the statistical error of the fit of the Stern-Volmer relation $\delta_{nf}^{\mathrm{fit}}$ and the estimated error due to uncertainty in MCS calibration $\delta_{nf}^{\mathrm{MCS}}$ were taken into account, combined as square root of the sum-of-the-squares. $\delta_{nf}^{\mathrm{MCS}}$ amounts to 1, 0.8, 0.6, and 0.5 %, for $n=5$, 6, 7, 8 nf states, respectively, while $\delta_{nf}^{\mathrm{fit}}$ amounts to 2.6, 2.8, 2.5, and 2.3 %, for $n=5,6,7,8$, respectively. Since corrections

TABLE IV. The lifetimes of the nf states of potassium atom.

State	Ref. [22]	Present work	
		Theory	Experiment
$5f$	126	117(4)	117(3)
$6f$	205	195(4)	190(6)
$7f$	314	301(6)	309(8)
$8f$	457	441(9)	428(10)

$\Gamma_{nf}^{\mathrm{BBR}}$ were small, as listed above, we believe that an error in calculation of the corrections, though not provided by the author of Ref. [22], should have negligible effect on our final τ_{nf} values, as well as an error introduced to these corrections by our interpolation procedure, and we disregarded these sources of uncertainty.

IV. RESULTS AND CONCLUSIONS

The experimental lifetimes together with the respective results of calculation described in Sec. II are listed in Table IV. We also list the theoretical values from Ref. [22] for comparison. We expect our theory values to be more accurate than the results from Ref. [22] owing to more complete treatment of the correlation correction. We find excellent agreement of the present theoretical results with the experimental measurements; the values for all states agree within the corresponding uncertainties.

In summary, we carried out both theoretical and experimental studies of the nf lifetimes in potassium. This work represents a benchmark test of the applicability of the all-order method for the calculation of the properties of such highly excited states and presents experimental potassium lifetimes for the nf states.

ACKNOWLEDGMENTS

The work of M.S.S. was supported in part by U.S.A. National Science Foundation Grant No. PHY-04-57078. The other authors acknowledge partial support by the EU-FP6-TOK project LAMOL (Contract No. MTKD-CT-2004-014228).

[1] J. K. Link, J. Opt. Soc. Am. **56**, 1195 (1966).
[2] R. W. Schmieder, A. Lurio, and W. Happer, Phys. Rev. **173**, 76 (1968).
[3] D. Zimmermann, Z. Phys. A **275**, 5 (1975).
[4] B. R. Bulos, R. Gupta, and W. Happer, J. Opt. Soc. Am. **66**, 426 (1976).
[5] U. Teppner and P. Zimmermann, Astron. Astrophys. **64**, 215 (1978).
[6] M. Głódź and M. Kraińska-Miszczak, J. Phys. B **18**, 1515 (1985).
[7] M. Głódź and M. Krainska-Miszczak, Phys. Lett. **110A**, 203 (1985).
[8] R. W. Berends, W. Kedzierski, J. B. Atkinson, and L. Krause, Spectrochim. Acta, Part B **43**, 1069 (1988).
[9] U. Volz and H. Schmoranzer, Phys. Scr. **T65**, 48 (1996).
[10] H. Wang, J. Li, X. T. Wang, C. J. Williams, P. L. Gould, and W. C. Stwalley, Phys. Rev. A **55**, R1569 (1997).
[11] A. Mills, J. A. Behr, L. A. Courneyea, and M. R. Pearson, Phys. Rev. A **72**, 024501 (2005).
[12] T. F. Gallagher and W. E. Cooke, Phys. Rev. A **20**, 670 (1979).
[13] D. P. Aeschliman, J. Quant. Spectrosc. Radiat. Transf. **25**, 221 (1981).
[14] L. N. Shabanova and A. N. Khlyustalov, Opt. Spectrosc. **59**, 123 (1985).
[15] D. J. Hart and J. B. Atkinson, J. Phys. B **19**, 43 (1986).
[16] P. F. Liao and J. E. Bjorkholm, Phys. Rev. Lett. **36**, 1543 (1976).
[17] J. Szonert, B. Bieniak, M. Głódź, and M. Piechota, Z. Phys. D: At., Mol. Clusters **33**, 177 (1995).
[18] P. E. Gruzdev and V. I. Denisov, Opt. Spectrosc. **52**, 8 (1982).
[19] A. Lindgard and S. Nielsen, At. Data Nucl. Data Tables **19**, 533 (1977).
[20] V. A. Zilitis, Opt. Spectrosc. **67**, 595 (1989).
[21] Xinghong He, Baiwen Li, Aiqiu Chen, and Chengxiu Zhang, J. Phys. B **23**, 661 (1990).
[22] C. E. Theodosiou, Phys. Rev. A **30**, 2881 (1984).
[23] W. R. Johnson, Z. W. Liu, and J. Sapirstein, At. Data Nucl. Data Tables **64**, 279 (1996).
[24] M. S. Safronova, W. R. Johnson, and A. Derevianko, Phys. Rev. A **60**, 4476 (1999).
[25] S. A. Blundell, W. R. Johnson, and J. Sapirstein, Phys. Rev. A **43**, 3407 (1991).
[26] J. A. Sherman, T. W. Koerber, A. Markhotok, W. Nagourney, and E. N. Fortson, Phys. Rev. Lett. **94**, 243001 (2005).
[27] M. S. Safronova, A. Derevianko, and W. R. Johnson, Phys. Rev. A **58**, 1016 (1998).
[28] W. R. Johnson, S. A. Blundell, and J. Sapirstein, Phys. Rev. A **37**, 307 (1988).
[29] M. Głódź, A. Huzandrov, J. Klavins, I. Sydoryk, J. Szonert, S. Gateva-Kostova, and K. Kowalski, Acta Phys. Pol. A **98**, 353 (2000).
[30] A. N. Nesmeyanov, *Vapor Pressure of the Chemical Elements* (Elsevier, Amsterdam, 1963).
[31] P. Hannaford and R. M. Lowe, Opt. Eng. **22**, 532 (1983).
[32] L. J. Curtis and P. Erman, J. Opt. Soc. Am. **67**, 1218 (1977).
[33] F. Gounand, M. Hugon, P. R. Fournier, and J. Berlande, J. Phys. B **12**, 547 (1979).
[34] Z. Kuprionis and V. Švedas, Appl. Phys. B: Lasers Opt. **59**, 649 (1994).
[35] L. R. Pendrill, J. Phys. B **10**, L469 (1977).
[36] G. W. Series, Comments At. Mol. Phys. **7**, 117 (1978).
[37] M. Głódź, A. Huzandrov, I. Sydoryk, J. Szonert and J. Klavins,Acta Phys. Pol. **A112**, 1185 (2007).